Simulation of Tsunamis in the East Sea Using Dynamically-Interfaced Multi-Grid Model

동적결합둥지형 모형에 의한 동해안 쓰나미 시뮬레이션

최 병 호* 에핌 페리놉스키** 우 승 범*** 이 종 웅**** 문 종 윤*****
Choi, Byung Ho Pelinovsky, Efim Woo, Seung Buhm Lee, Jong Woong Mun, Jong Yoon

국문요약

상세한 지진해일 범람 현상을 규명하기 위하여 수립된 전회의 동적결합 차분 모형(Choi et al.[1])이 1983년 동해중부지진에 의한 지진해일 연구를 위해 우리나라 동해안 전역에 적용되었다. 계산영역은 격자의 크기가 다른 몇 개의 둥지영역이 평행하거나 경사가 진 방향으로 연결되어 구성되어 있다. 제일 안쪽의 둥지 영역은 해안을 따라 순차적으로 16영역으로 구성되었으며, 격자간격은 약 30m이다. 천수방정식(선형과 비선형)이 적용된 수치 시뮬레이션은 둥지영역의 격자크기에 따라 직각 또는 구면좌표계가 채택되었으며, 평행 및 경사 접합이 제일 안쪽의 둥지형 모형에 적용되었다. 시뮬레이션에 의한 결과는 지진해일 사상에 대한 처오름 높이의 관측치와 잘 일치하였다. 지진해일고 분포곡선의 개선이 수치적으로 연구되었으며, 지진원으로부터 거리가 먼 경우에는 대수정규분포를 따르는 경향을 보인다.

주요어 : 지진해일, 동적결합둥지형모형, 처오름, 분포곡선

ABSTRACT

A dynamically-interfaced multi-grid finite difference model for simulation of tsunamis in the East Sea(Choi et al.[2]) was established and further applied to produce detailed feature of coastal inundations along the whole eastern coast of Korea. The computational domain is composed of several sub-regions with different grid sizes connected in parallel or inclined directions with 16 innermost nested models. The innermost sub-region represents the coastal alignment reasonably well and has a grid size of about 30 meters. Numerical simulations have been performed in the framework of shallow-water equations(linear, as well as nonlinear) over the plane or spherical coordinate system, depending on the dimensions of the sub-region. Results of simulations show the general agreements with the observed data of run-up height for both tsunamis. The evolution of the distribution function of tsunami heights is studied numerically and it is shown that it tends to the log-normal curve for long distance from the source.

Key words : tsunami, dynamically-interfaced multi-grid model, run-up, distribution function

1. Introduction

In historical point of view, Japanese and Russian coastal region adjacent to the East Sea(Fig. 1) have suffered from tsunamis more severely than Korean coast has. However the tsunami hazard along eastern coast of Korea should not be ignored, since tsunami outbreak in the East Sea is not a rare event anymore. There have been moderate and strong tsunamis during last century in the East(Japan) Sea; August 2, 1940(Shakotan-Oki earthquake); May 7, 1964 (Niigata earthquake); May 26, 1983(East Sea central region earthquake) and July 12, 1993(Southwest off Hokkaido earthquake). Earthquake sources are located along the Japanese coast on the possible boundary between the Eurasian and the North American plates. The earthquake of May 26, 1983 is the one of the strongest earthquakes ever happened in this source region. A tsunami followed, and its highest run-up was measured at more than 15m above MSL along the Japanese Coast. Tsunami propagated across the East Sea and damaged middle part of eastern coast of Korea, especially inundating ports of Mukho and Imwon. Previously this event tsunamis in the eastern coast of Korea usually were considered as a negligible coastal disaster.

This paper presents numerical hindcasting studies on the 1983 tsunami events using multi-grid, dynamically-interfaced finite difference model and shows the log-normal distribution pattern of tsunami run-up height along the coastline in each innermost sub-region. A fine mesh(30meters or so) is used in the innermost sub-region along the coastline, which is connected to outer region either parallel or inclined directions. This was necessary due to the characteristic behavior of tsunamis in the eastern coast of Korea, which is significantly influenced by bottom topography and irregular coastline of the East Sea.

The present work is an extension of the previous study (Choi et al.[1]), where only two innermost subregions covering middle and southern coast of Korea are investigated. In

* 정회원·성균관대학교 토목환경공학과, 정교수
(대표저자 : bhchoi@yurim.skku.ac.kr)
** 러시아 과학원 응용물리연구소, 교수
*** 미국 코넬대학교 토목환경공학과, 박사후과정
**** 성균관대학교 토목환경공학과, 석사과정수료
***** 성균관대학교 토목환경공학과, 석사과정
본 논문에 대한 토의를 2003년 4월 30일까지 학회로 보내 주시면 그 결과를 게재하겠습니다. (논문접수일 : 2002. 12. 3 / 심사종료일 : 2003. 1. 24)

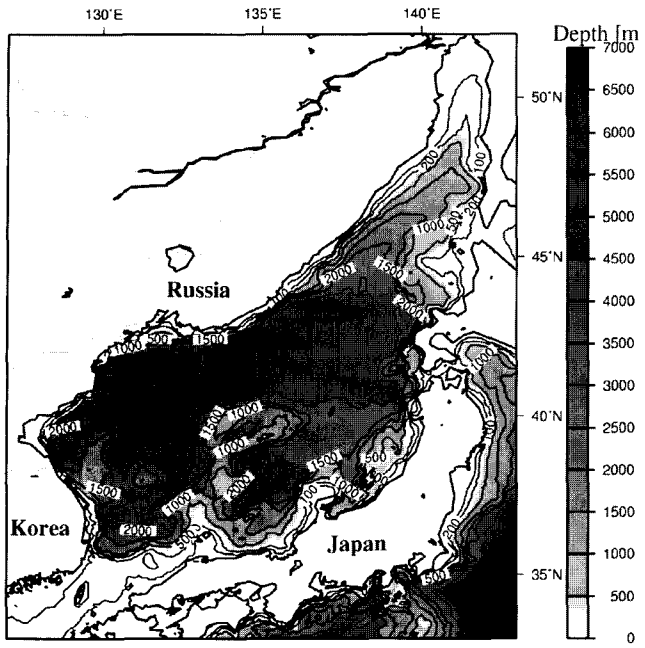

Fig. 1 Bathymetry of the East Sea

this work a total of 16 innermost subregions covering the whole eastern coast of Korea are studied. In each sub-region, the comparison of numerical results with log-normal distribution function is made.

The paper is organized as follow. The numerical model is described in section 2. The choice of the basic equations depends on the size of modeled area and either cartesian or spherical coordinate system is applied accordingly. Typically, spherical linear model is used for the large area in the open ocean, whereas cartesian nonlinear model with moving boundary and friction is applied to the coastal zone. Algorithms for dynamic interfacing are described. Numerical results for the 1983 event are given in section 3. They are compared with observed data. Also the evolution of the distribution function of the wave heights with distance is investigated. It is shown that the distribution function tends to the log-normal curve for long distance from the source.

2. Numerical model

2.1 Basic equations

For a tsunami propagating in deep ocean, both the frequency dispersion and Coriolis force can play important roles. On the other hand, the wave steepness of this distant tsunami is so small that the nonlinear convective inertia force can be ignored. As tsunamis propagate into the shallow-water region, the wave amplitude increases and the wavelength decreases due to shoaling. The nonlinear convective inertia force becomes increasingly important, which are discussed by Murty[2] and Pelinovsky.[3] In the very shallow water, the bottom frictional effects become significant, while the significance of the frequency dispersion diminishes. Therefore, the nonlinear shallow-water equations including bottom frictional terms should be used in the description of the tsunami run-up. The multi-grid coupled finite difference model is constructed to simulate the whole process of tsunami generation, propagation and run-up. In the model, either the linear or the nonlinear version of the shallow-water equation with different type of coordinate system(i.e. Cartesian or Spherical) can be assigned to a specific region. These sub-regions are dynamically connected and any ratio of grid sizes can be used for the connection of two adjacent sub-regions. The entire computational domains are divided into four sub-regions(Fig. 2(a)) for parallel connecting scheme and five sub-regions(Fig. 2(b)) for inclined connecting scheme. Fig. 3 shows the total 16 innermost subregions studied in this work, which covers the entire

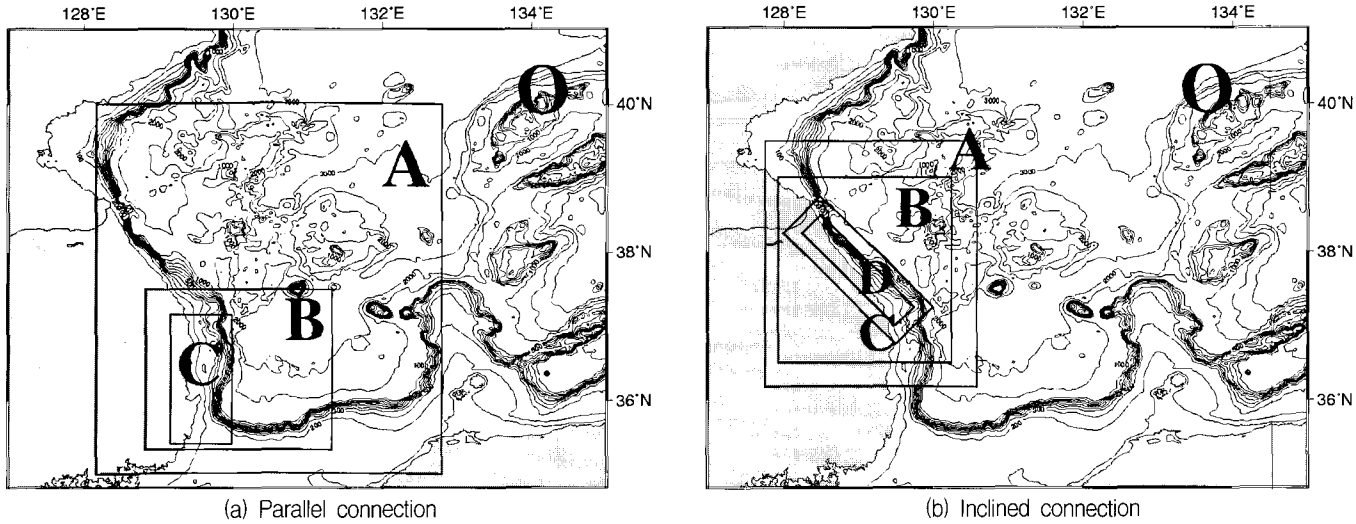

(a) Parallel connection (b) Inclined connection

Fig. 2 Nested grid system of the finite difference tsunami model for the East(Japan) sea shown over the bathymetry of the region

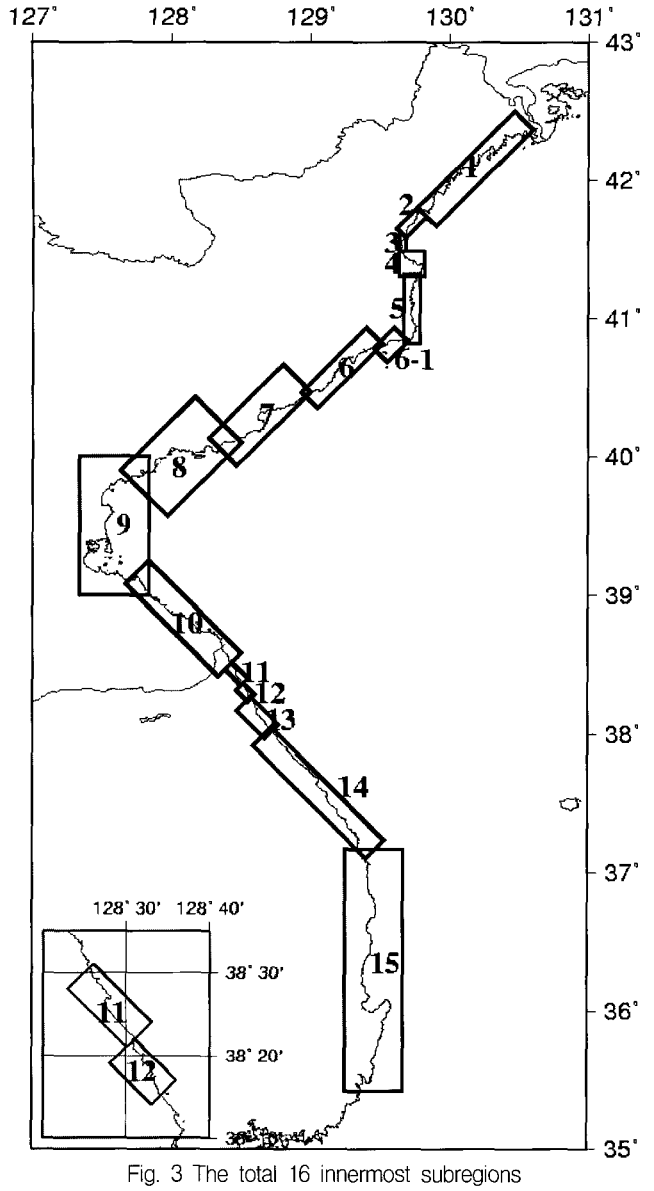

Fig. 3 The total 16 innermost subregions

eastern coastline of Korea. As it is shown in the figure, the irregular geometry of coastline can be adequately covered by innermost subregions through the combination of either parallel or inclined connection.

Each sub-region uses its own time-step, spatial grid size, coordinates and governing equations. Coordinates and governing equations for each region are,

- Region O : covering the whole computational area(the East Sea), the mesh size is 1minute and the time step 2sec. The spherical coordinates and linear shallow-water equations are used as:

$$\frac{\partial \zeta}{\partial t}+\frac{1}{R\cos\phi}\left[\frac{\partial P}{\partial \chi}+\frac{\partial}{\partial \phi}(Q\cos\phi)\right]=0$$
$$\frac{\partial P}{\partial t}+\frac{gh}{R\cos\phi}\frac{\partial \zeta}{\partial \chi}-fQ=0$$
$$\frac{\partial Q}{\partial t}+\frac{gh}{R}\frac{\partial \zeta}{\partial \phi}+fP=0 \qquad (1)$$

In equations above, ζ is an elevation of the sea surface above the undisturbed level, ϕ and χ are the latitude and longitude(x and y are projections of ϕ and χ), P and Q are the discharges per unit width in the direction of ϕ and χ, respectively, h is the undisturbed level, H is the total depth of water($H=h+\zeta$), R is the radius of the earth, g is the acceleration of gravity, τ_x, τ_y are the bottom frictions, f is the Coriolis parameter.

- Region A : the mesh size is 0.333 minute and the time step 1sec. The spherical coordinates and linear shallow-water Eq. (1) are used.
- Region B :
  - for parallel connection, the mesh size is 125m and the time step 0.5sec;
  - for inclined connection, the mesh size is 150m and the time step 0.5sec;
  - For both cases the Cartesian coordinates and linear shallow-water equations are used as:

$$\frac{\partial \zeta}{\partial t}+\frac{\partial P}{\partial x}+\frac{\partial Q}{\partial y}=0$$
$$\frac{\partial P}{\partial t}+gh\frac{\partial \zeta}{\partial x}=0$$
$$\frac{\partial Q}{\partial t}+gh\frac{\partial \zeta}{\partial y}=0 \qquad (2)$$

- Regions C : for parallel connection, mesh size is 25m and time step 0.25sec.

The Cartesian coordinates and nonlinear shallow-water equations with moving boundary and bottom friction(=0.013) are used as:

$$\frac{\partial \zeta}{\partial t}+\frac{\partial P}{\partial x}+\frac{\partial Q}{\partial y}=0$$
$$\frac{\partial P}{\partial t}+\frac{\partial}{\partial x}\left(\frac{P^2}{H}\right)+\frac{\partial}{\partial y}\left(\frac{PQ}{H}\right)+gh\frac{\partial \zeta}{\partial x}+\tau_x H=0$$
$$\frac{\partial Q}{\partial t}+\frac{\partial}{\partial x}\left(\frac{PQ}{H}\right)+\frac{\partial}{\partial y}\left(\frac{P^2}{H}\right)+gh\frac{\partial \zeta}{\partial y}+\tau_y H=0 \qquad (3)$$

For inclined connection, the mesh size is 106.066m and the time step 0.25sec.

The Cartesian coordinates and linear shallow-water Eq. (2) are used for this area.

- Regions D : For inclined connection. The mesh size is 35.355m and time step 0.125sec. The Cartesian coordinates and nonlinear shallow-water equations with moving boundary and bottom friction (3) are used for this area.

As seen here, the ratio of the grid size between region O

and region A is 1:3, that of region A and region B is 1:4 for both schemes. For parallel connection, the ratio of grid the size between region B and region C is 1:5, and for inclined connection, $1:\sqrt{2}$. Between regions C and D the ratio is 1:3. The connecting boundary scheme is applied to the interfacial boundary so that adjacent two sub-regions are dynamically coupled. The outer(lateral) boundary of region O is treated as a radiated open boundary.

2.2 Numerical scheme

In the present work, the second order explicit leap-frog finite difference scheme is used for the discretization of linear terms in the governing equations over the staggered grid system. The finite difference equations for the linear shallow equations are proposed as(Abbott et al.[4]):

$$\frac{\zeta_{i,j}^{n+1/2}-\zeta_{i,j}^{n-1/2}}{\Delta t}+\frac{P_{i+1/2,j}^{n}-P_{i-1/2,j}^{n}}{\Delta x}+\frac{Q_{i,j+1/2}^{n}-Q_{i,j-1/2}^{n}}{\Delta y}=0 \tag{4}$$

$$\frac{P_{i+1/2,j}^{n+1}-P_{i+1/2,j}^{n}}{\Delta t}+gh\frac{\zeta_{i+1,j}^{n+1/2}-\zeta_{i,j}^{n+1/2}}{\Delta x}+\frac{rgh}{12\Delta x}[(\zeta_{i+1,j+1}^{n+1/2}-2\zeta_{i+1,j}^{n+1/2}+\zeta_{i+1,j-1}^{n+1/2})-(\zeta_{ij+1}^{n+1/2}-2\zeta_{i,j}^{n+1/2}+\zeta_{i,j-1}^{n+1/2})]=0 \tag{5}$$

$$\frac{Q_{i,j+1/2}^{n+1}-Q_{i,j+1/2}^{n}}{\Delta t}+gh\frac{\zeta_{1,j+1}^{n+1/2}-\zeta_{i,j}^{n+1/2}}{\Delta y}+\frac{rgh}{12\Delta y}[(\zeta_{i+1,j+1}^{n+1/2}-2\zeta_{i,j+1}^{n+1/2}+\zeta_{i-1,j+1}^{n+1/2})-(\zeta_{i+1,j}^{n+1/2}-2\zeta_{i,j}^{n+1/2}+\zeta_{i-1,j}^{n+1/2})]=0 \tag{6}$$

The last term in the momentum equations is included in order to improve the frequency dispersion relationship using the numerical dispersion caused by truncation error of the finite difference equations. Fig. 4 shows a grid system in which the free surface displacement is calculated at the center and the volume fluxes are obtained at the surrounding grid points. From the continuity equation, the free surface displacement, i.e., $\zeta_{i,j}^{n+1/2}$, at the (i, j) grid point on the (n+1/2))-th time step is calculated. The momentum equations are then used to calculate the volume flux components, $P_{i+1/2,j}^{n+1}$ and $Q_{i,j+1/2}^{n+1}$, at the (i+1/2, j) and (i, j+1/2) grid point, respectively, on the (n+1)-th time step. Therefore, time integration scheme adopted here is second order explicit. Note that the calculations for the free surface displacement and the volume flux components are staggered in time as well as in space. The upwind difference scheme is used for the convective terms in the nonlinear shallow water momentum equations. The bottom friction is modeled by using Manning's formula. The finite difference schemes for convective terms and the treatment of open and moving boundary conditions are the same as those used in Liu et al.[5] The detailed discussion on the treatment of connecting boundary will be given in section 2.4.

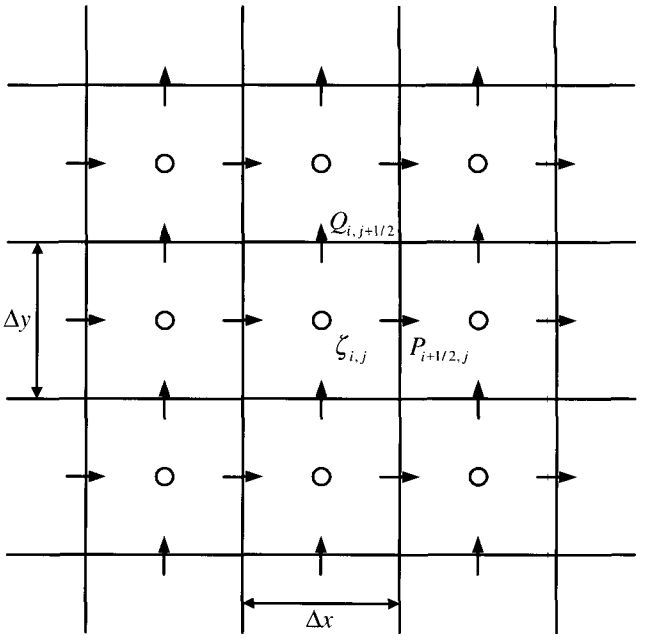

Fig. 4 The staggered finite difference grid system

2.3 Moving boundary treatment

In carrying out numerical computations, the computational domain is divided into finite difference grids. Initially, the free surface displacement is zero everywhere, as are the volume fluxes. When the grid point is on dry land, the "water depth," h, takes a negative value and gives the elevation of the land measured from the mean water level. Fig. 5 shows a schematic sketch of the moving boundary treatment used in the study(Liu et al.[5], Cho and Yoon[6]). The SWL represents the mean water level and H_f denotes the flooding depth in Fig. 5. In a land(dry) cell the total depth, $H=h+\zeta$, has a negative value. On the other hand, the wet cell has a positive H value. The interface between the dry cells and wet cells defines the shoreline. The continuity equation in conjunction with boundary conditions along offshore boundaries is used to find free surface displacements at the next time step in the entire computational domain, including the dry(land) cells. The free surface displacement at a dry land grid remains zero because the volume fluxes are zero at the neighboring grid points. At a shoreline grid, the total depth, H, is updated. A numerical algorithm is needed to determine if the total water depth is high enough to flood the neighboring dry

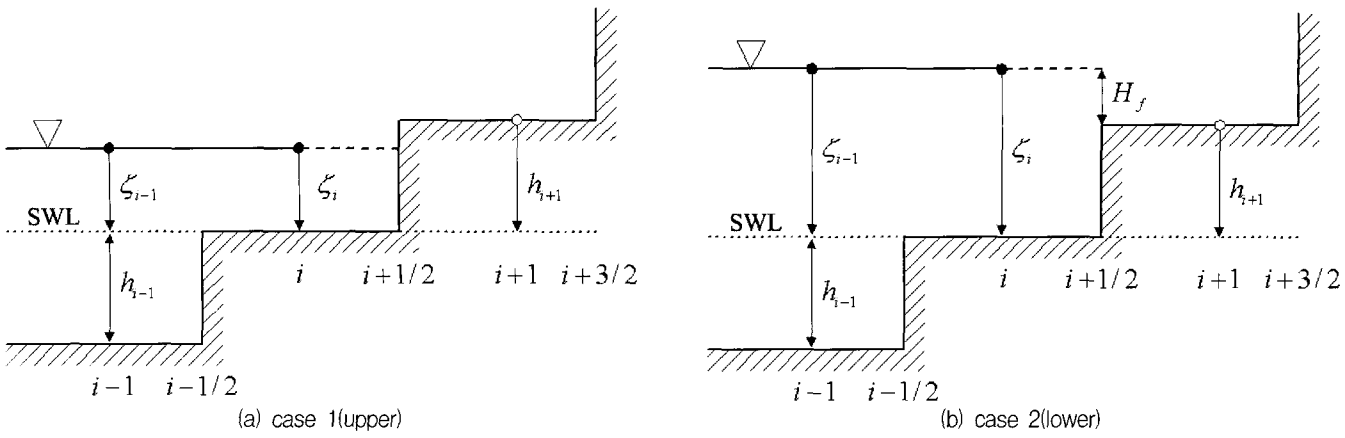

Fig. 5 A schematic sketch of the moving boundary treatment

(land) cells and hence to move the shoreline. The momentum equations are used to update the volume fluxes in the wet cells only. To illustrate the moving boundary algorithm, the one-dimensional case is used as an example. As shown in Fig. 5, the real bathymetry has been replaced by a staircase representation. The total depth, H, is calculated and recorded at grid points $i-1$, i and $i+1$, while the volume flux is computed at grid points $i-1/2$, $i+1/2$ and $i+3/2$. As shown in Fig. 5(a), the i-th cell is a wet cell in which the total depth is positive and the $(i+1)$-th cell is a dry(land) cell in which the total depth is negative and the volume fluxes are zero. The shoreline is somewhere between the i-th and the $(i+1)$-th grid points. Then, the volume flux at the $(i+1/2)$-th grid point is assigned to be zero. Therefore, the shoreline does not move to the on-shore direction. When the water surface is rising as shown in Fig 5(b), however, the volume flux at the $(i+1/2)$-th grid point is no longer zero. The shoreline may move one grid point to the on-shore direction. After the total depth has been updated from the continuity equation, the following algorithm is used to determine whether or not the shoreline should be moved. If $H_i > 0$, possible cases can be summarized as,

- if $H_{i+1} \le 0$ and $H_{i+1} + \zeta_i \le 0$, then the shoreline remains between grid points i and $i+1$ and the volume flux $P_{i+1/2}$ remains zero
- if $H_{i+1} \le 0$ and $H_{i+1} + \zeta_i > 0$, then the shoreline moves to between grid points $i+1$ and $i+2$. The volume flux $P_{i+1/2}$ may have a nonzero value, while $P_{i+2/3}$ is assigned to be zero. The flooding depth is $H_f = h_{i+1} + \zeta_i$
- if $H_{i+1} > 0$, then the shoreline moves to grid points between $i+1$ and $i+2$. The volume flux $P_{i+1/2}$ may also have a nonzero value, while $P_{i+2/3}$ has a zero value. The flooding depth is $H_f = \max(h_{i+1} + \zeta_i, h_{i+1} + \zeta_{i+1}$ $H_f = \max(h_{i+1} + \zeta_i, h_{i+1} + \zeta_{i+1})$

In the above cases, the time-step index has been omitted for simplicity. The algorithm is developed for a two-dimensional problem and the corresponding y-direction algorithm has the same procedure as that for the x-direction. To save computing time, the regions that represent permanent dry(land) can be excluded from the computation by installing a depth criterion. Moreover, when H is very small, the associated bottom friction term become very large and, accordingly, a lower bound of the water depth is used to avoid the difficulty. The finite difference approximation for the continuity equation correctly accounts for positive and zero values of the total depth on each side of a computational grid. The treatment of flooding and ebbing grid cells guarantees mass conservation while accounting for the flooding and ebbing of land. The occurrence of a zero value for the total depth H on one side of a cell implies zero mass flux until H becomes positive. A grid cell is considered, as dry cell only if the total water depths at all sides are zero or negative.

2.4 Algorithm for dynamic interfacing

2.4.1 Parallel connecting boundary condition

We briefly describe the technique for exchanging information between two sub-regions of different grid sizes. As shown in Fig. 6, a smaller grid system is nested in a larger grid system with the ratio of 1:3. The arrows represent the volume fluxes, P and Q, across each grid cell, while circles and dots indicate the locations where the free surface displacement is evaluated.

At a certain time level, volume fluxes in both large and small grid systems are determined from the momentum equations, with the exception of volume fluxes for the smaller grid system along the boundaries between two sub-regions. These data are determined by interpolating the neighbouring volume fluxes from the large grid system.

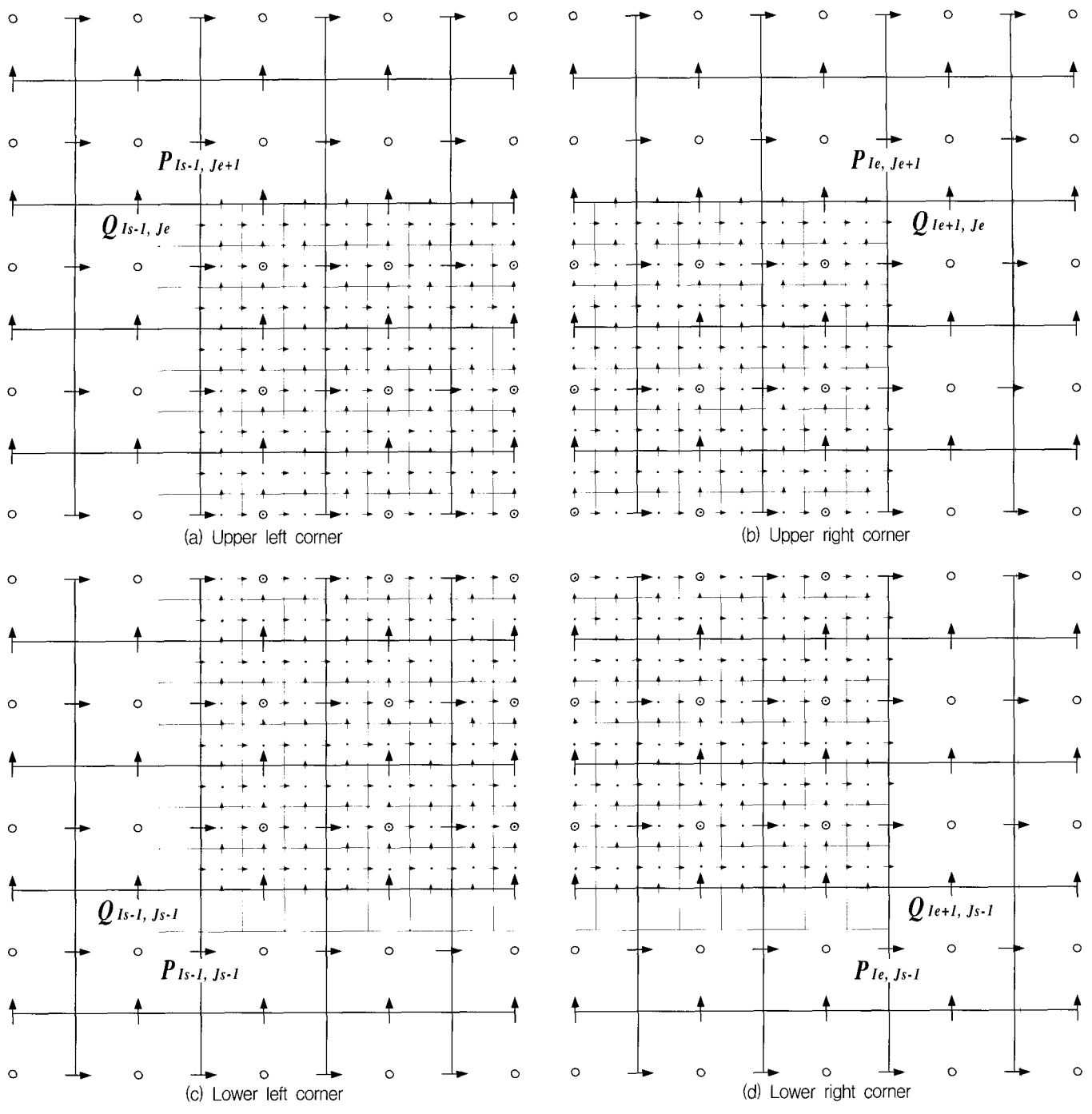

Fig. 6 Parallel connecting boundary between two subregions

The free surface displacement at the next time level for the small grid system can be calculated from the continuity equation. Usually the time step size for the smaller grid system is also smaller than that used in the larger grid system to satisfy the Courant-Friedrichs-Lewy condition, which is $c\Delta t/\Delta tx<1$. Therefore, the volume fluxes along the boundary of the small grid system at the next time level must be obtained by interpolating the neighbouring volume fluxes obtained from the large grid system over a larger time interval. After the free surface displacements in the small grid system are calculated up to the next time level of the large grid system, the free surface displacements in the large grid system are updated by solving the continuity equation.

Let us describe these procedures step by step. Fig. 7 shows the time axis for the outer grid (t_{out}) and the inner grid (t_{in}). The circle and the cross represent the time step at which free surface elevation and volume fluxes are calculated, respectively. It is noted that the time step size of outer grid is twice as large as that of inner grid. Suppose all flux values in the inner and the outer region are known at time level $t=t^n$. And now we need to solve the inner and the outer region values at the next time step.

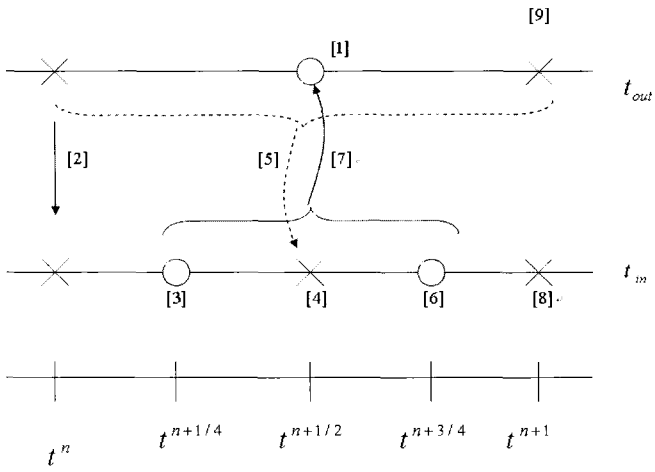

Fig. 7 The time axis for outer grid(t_{out}) and the inner grid(t_{in})

(1) Obtain the free surface elevation at $t^{n+1/2}$ in the outer region by solving continuity equation.

(2) To solve the continuity in the inner region, however, we need to have the flux information along the connected boundary at t^n. So the flux values in the outer grid at the connected boundary are linearly interpolated and then those interpolated values are assigned to the flux in the inner grid at the boundary.

(3) Obtain the free surface elevation at $t^{n+1/4}$ in the inner region by solving continuity equation.

(4) Obtain the flux values at $t^{n+1/2}$ in the inner region by solving momentum equation.

(5) To obtain the free surface elevation at $t^{n+3/4}$ in the inner region, we should have the flux information along the connected boundary at $t^{n+1/2}$. To get this information we can do in following way. First, since we already know the free surface elevation at $t^{n+1/2}$ and flux at t^n in the outer region, the flux in the outer region along the connected boundary at t^{n+1} can be obtained by solving linear momentum equation locally. This can be regarded as a predicted value of flux at t^{n+1}. Second, the outer flux values at t^n and t^{n+1} are time averaged to get outer flux values at $t^{n+1/2}$. And these values are linearly interpolated along the connected boundary. Those spatially and timely averaged flux values are assigned to the flux in the inner grid at the boundary.

(6) Obtain the free surface elevation at $t^{n+3/4}$ in the inner region by solving continuity equation.

(7) To transfer the information from the inner region to the outer region, the free surface elevation in the inner region is spatially averaged over the grid size of the outer region. These spatially averaged elevation values at $t^{n+3/4}$ are then time averaged with those at $t^{n+1/4}$ in inner region. These spatially and timely averaged elevation values in the inner region update the elevation values at $t^{n+1/2}$ in the outer region.

(8) Obtain the flux values at t^{n+1} in the inner region by solving momentum equation.

(9) Obtain the flux values at t^{n+1} in the outer region by solving momentum equation. This can be regarded as a corrected value of outer flux at t^{n+1}.

By iterating from step (5) to (9) until the difference between two iterated values is smaller than the error criteria, the converged solution of inner and outer flux across the connecting boundary can be obtained. In our experience, however, this additional iteration is not necessary when the non-linearity is small.

2.4.2 Inclined connecting boundary condition

When the coastline in the region of interest is slanted, it is difficult to represent the accurate coastline with the finite difference grid system unless the grid size is relatively small. If the coastline is not much indented, it can be more accurately represented by rotating the axis of grid system to be parallel to the coastline. A new method is developed for dynamically connecting the rotated sub-region with the outer grid system(Fig. 8).

At this stage, the inclined connecting boundary condition method can be used for the Cartesian grid system with linear governing equations.

The ratio of grid sizes between the inner fine grid and outer coarse grid is in the ratio of $1:\sqrt{2}$ and fixed. The time step size in inner grid system should be same as that of the outer grid system. ($dt_c = dt_f$). The general procedure for inclined connecting boundary condition method is shown below.

(1) Obtain the free surface elevation at $t^{n+1/2}$ in the inner and outer region by solving continuity equation, respectively.

(2) The calculated free surface elevation in inner and outer region is exchanged through interpolation at $t^{n+1/2}$.

(3) Obtain the flux values at t^{n+1} in the inner and outer region by solving momentum equation with the exchanged free surface elevation.

(4) The calculated flux values in inner and outer region are exchanged through interpolation at t^{n+1}.

2.4.3 Numerical experiments

To examine the connecting boundary condition, numerical

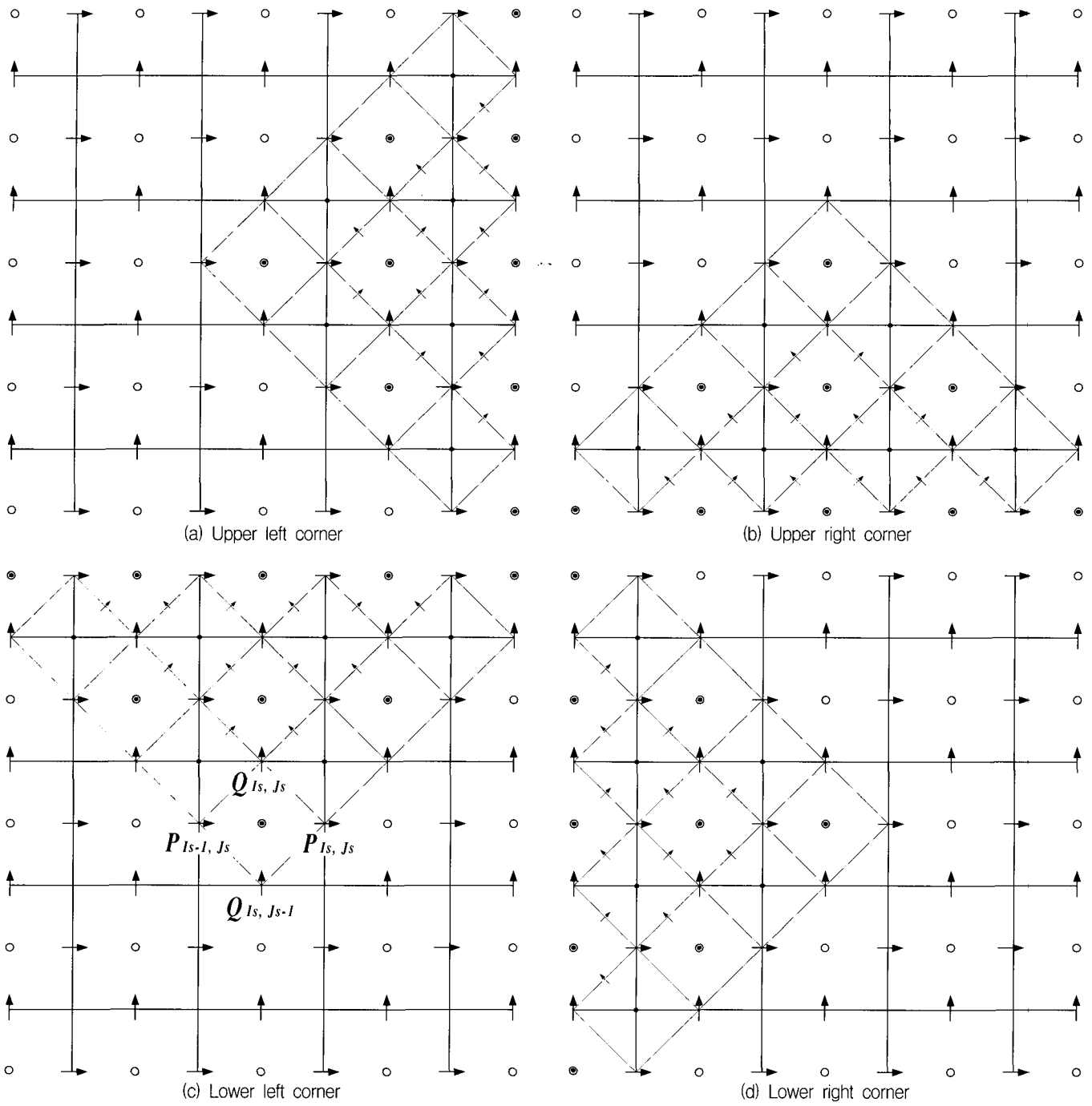

Fig. 8 Inclined connecting boundary between two subregions

experiments to test the nested model by checking the propagation and the reflection of tsunami wave across the connecting boundary were performed. A sequence of snap-shots of free-surface displacement for the propagation of tsunami wave across the connecting boundaries placed in parallel and inclined manner, are shown Figs. 9 and 10. It is seen that the wave propagation is smooth and that there is no significant numerical error when the wave across the boundaries of four regions of different grid resolution, suggesting the connecting boundary condition seems to exchange the information between two adjacent regions very well.

2.5 Fault parameters for source region

Among the several fault parameters of the 1983 Central East Sea earthquake, the Aida Model-10 is now considered as the best estimate, because it explains well the total tsunami energy and the distribution of tsunami energy. Table 1 shows the accepted fault parameters by Aida Model-10(Aida[7]).

The initial surface profile is determined by the method of Manshinha and Smylie[8], which assumes that the initial surface profile is the same as the movement of vertical dislocation of sea-bed when the speed of vertical dislocation

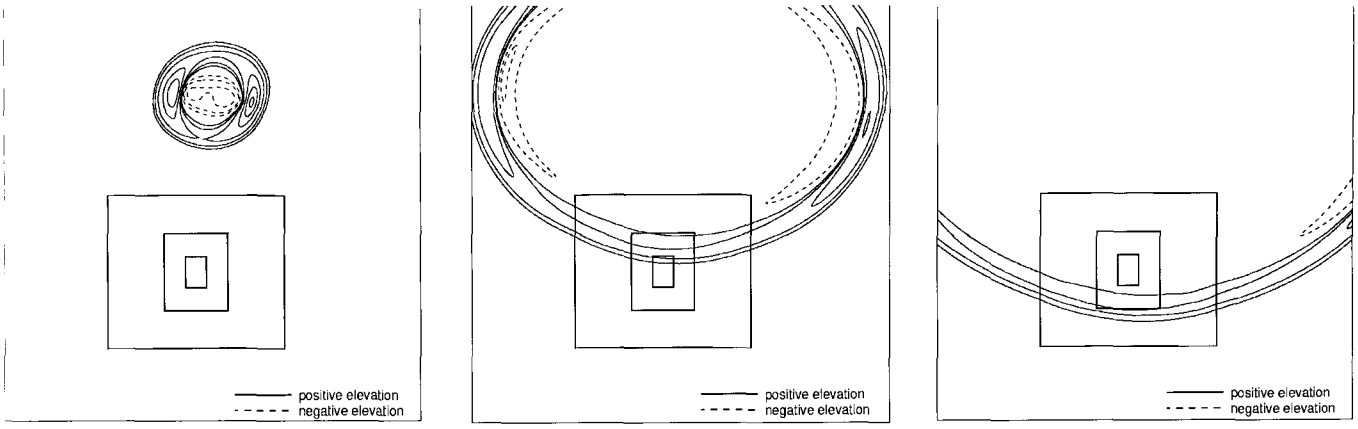

Fig. 9 Tsunami wave propagation of parallel connecting scheme

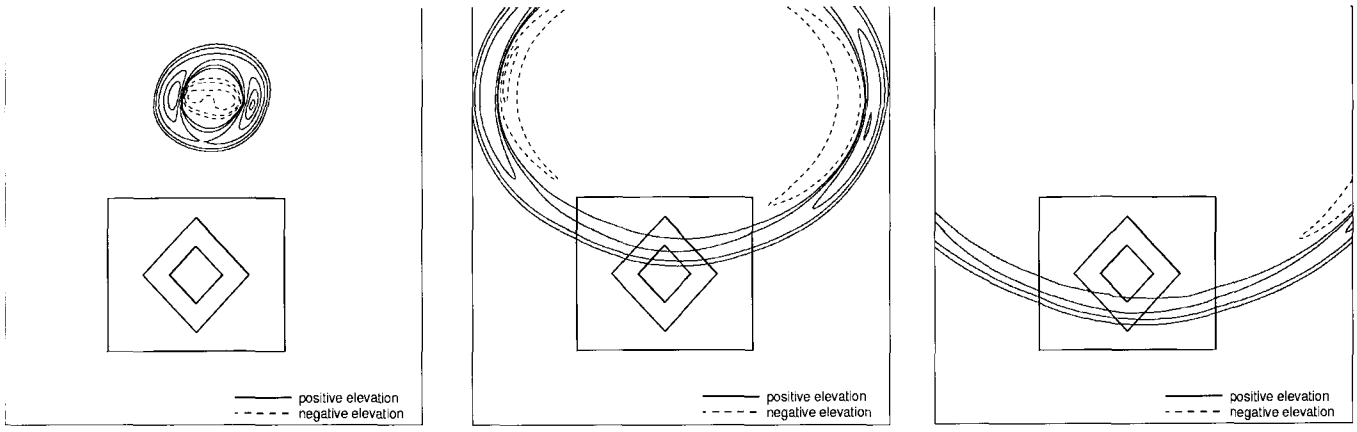

Fig. 10 Tsunami wave propagation of inclined connecting scheme

Table 1 Fault parameters of the 1983 Central East Sea earthquake

N(°N)	E(°E)	H(km)	θ(°)	δ(°)	λ(°)	L(km)	W(km)	U(cm)
40.21	138.84	2	22	40	90	40	30	760
40.54	139.02	3	355	25	80	60	30	305

where N : longitude(°N), E : latitude(°E), H : focal depth(km), θ : strike angle(°), δ : dip angle(°), λ : slip angle(°), L : length(km), W : width(km) U : dislocation(cm)

of plate is faster than the celerity of the propagation of the long wave. Fig. 9 shows the estimated fault dislocation of the 1983 Central East Sea earthquake corresponding the initial sea surface profile.

2.6 Bathymetry and coastal-topography data

We have compiled all the available topographic data along with digitization of hydrographic charts including Chinese and Russian navigation charts and Korean hydrographic charts to produce 1 minute gridded topography and bathymetry dataset for the region 117°~143° East longitudes and 24°~52° North latitudes. A certain effort was made to correct depths at chart datum to local MSL and then smoothing algorithm was applied to remove discontinuity arising from different region of charts. Topography data sampled at 1-minute interval was taken from USGS GTOPO30 dataset, which has approximately 1-kilometer resolution(30arcsec). This one minute gridded topographic and bathymetric dataset created in the present study could suffice for modeling of tsunamis propagation over the distant source, which is the most oceanographic problem. However, tsunami phenomenon and storm surge inundation modeling at coastal region require more detailed coastal topography and bathymetry at shoreline boundaries.

Another laborious work digitizing the coastal bathymetric map(1:25,000 scale map from NGI(National Geographic Institute) and KIGAM(Korea Institute of Geoscience and Mineral Research) charts for offshore region, respectively) were performed and merged with DEM dataset to produce 1 arcsecond(about 30m) gridded topographic and bathymetric dataset for southern Korea and neighbouring coastal area (Fig. 10). The mentioned charts from NGI, KIGAM have been prepared during last 20 years or so, therefore they

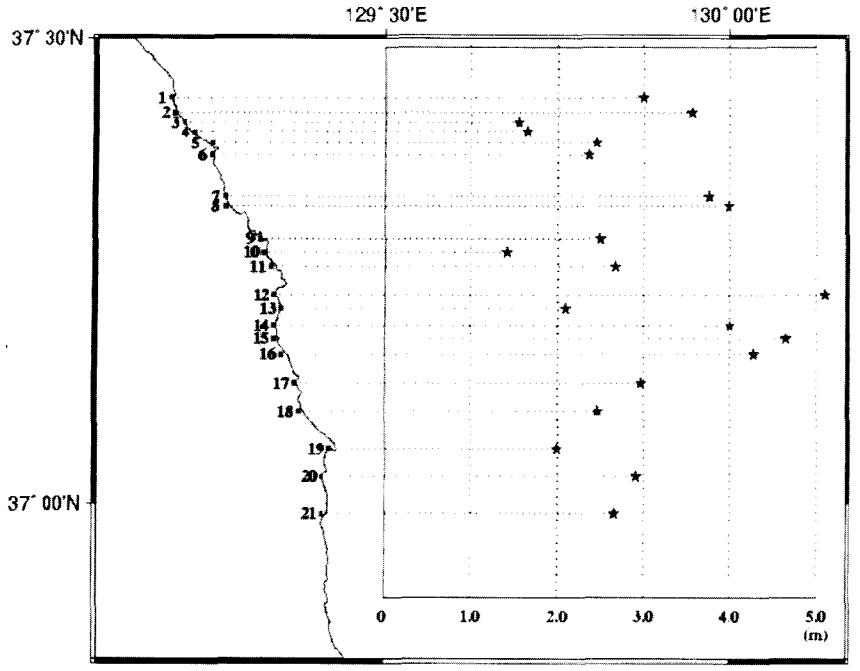

Tsunami Heights

Name of points	Height(meter)
1. Samchuk Port	2.99
2. Geunduk	3.56
3. Namapo	1.55
4. Gungchun Beach	1.65
5. Gungchun	2.46
6. Chogok	2.36
7. Yongwha Beach	3.76
8. Yongwha Port	3.99
9. Jangho Port	2.50
10. Galnam Port	1.42
11. Shinnam Port	2.67
12. Imwon Port	5.10
13. Biwha Port	2.09
14. NogokPort	4.00
15. Jakjin Port	4.65
16. Hosan Port	4.28
17. Nagok Port	2.97
18. Bugu Port	2.47
19. Chukbyun Port	1.99
20. Onyang Port	2.91
21. Eubnam Port	2.66

Fig. 11 Observed tsunami run-up height along the east Korean coast for the 1983 tsunami event(NIDP[9])

may not reflect local depth changes correctly due to strong dynamic sedimentation regime around Korean coast. Mapping of coastline over the large sea area around the Korean Peninsula also renders the problem of positional accuracy. Detailed tsunami and storm surge inundation modeling requires more detailed coastline information in terms of positional accuracy and shape of coastline and so on. In the present study, the grid system used for inner coastal area for inundation was chosen as 30meter grid-length.

3. Numerical results and discussion

The Developed numerical method is used to simulate the manifestation of tsunami in East Sea in 1983 on the Korean coast. This event is provided by the observed data of run-up heights and time of appearance of the tsunami. The 1983 Central East Sea earthquake has induced the tsunami waves flooded the Japanese, Korean and Russian coasts of the East Sea. The post tsunami run-up survey at the east Korean coast due to this 1983 tsunami event were performed by Japanese Disaster Prevention Research Institute with the assistance from the Office of Hydrographic Affairs and the Korea Meteorological Administration(Tsuji et al.[9]) but the survey was limited in terms of run-up heights measurement. NIDP[10] performed re-investigation for this event and gathered tsunami run-up heights at 24 points. Results of the updated measured wave heights in 21 coastal points along the eastern coast of Korea are presented in Fig. 11. The wave height varies from the minimal value of 1.42m(Galnam Port) to the maximal value of 5.1m and 7.5m(Port of Imwon and up reach of the river). As usual, the variation of the wave height is related with the features of the bottom and coastal relief. More convenient to present observed data is to use the distribution function of tsunami heights. Due to random bottom topography, the density of the distribution function should be described by log-normal curve(Van Dorn[11], Kajiura[12], Choi et al.[13]).

$$f(H)=\frac{1}{H\sigma\sqrt{2\pi}\ln 10}\exp\left(-\frac{(\log H-a)^2}{2\sigma^2}\right) \qquad (7)$$

Where H is the maximal value of run-up height for each coastal point in meters, a is a mean value of $\log H$ and σ

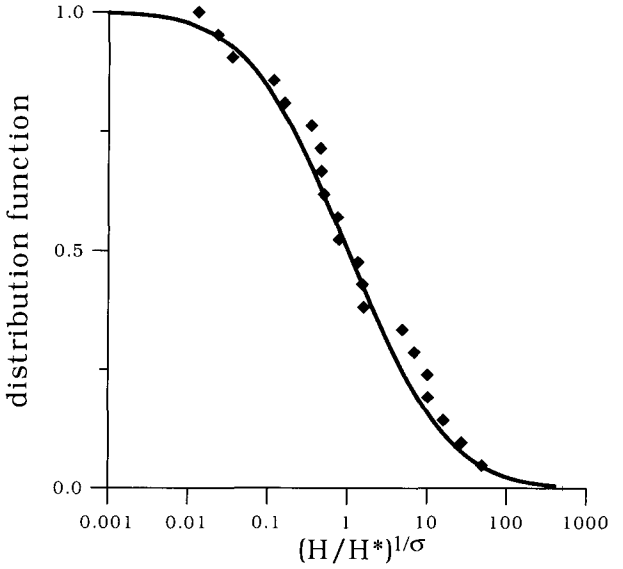

Fig. 12 Distribution function of tsunami heights along the east Korean coast, May 26, 1983(comparision with observed data)

is the standard deviation of $\log H$. For observed data of the 1983 tsunami presented in Fig. 11 parameters of the distribution are: a=0.454 and σ=0.152. The distribution function obtained by integrating (7) can be presented in the universal form(Choi et al.[13]).

$$f(\zeta)=\frac{1}{\sqrt{2\pi}\ln 10}\int_{\zeta}^{\infty}\exp\left(-\frac{1}{2}(\log\theta)^2\right)\frac{d\theta}{\theta} \qquad (8)$$

Where,

$$\zeta=\left(\frac{H}{\overline{H}}\right)^{1/\sigma}, \qquad \overline{H}=10^{a} \qquad (9)$$

and this is convenient to compare data of different tsunamis. The distribution function for the 1983 tsunami obtained on observed data is given in Fig. 12. Here the solid line is the theoretical curve (8) and dotts are the obtained from

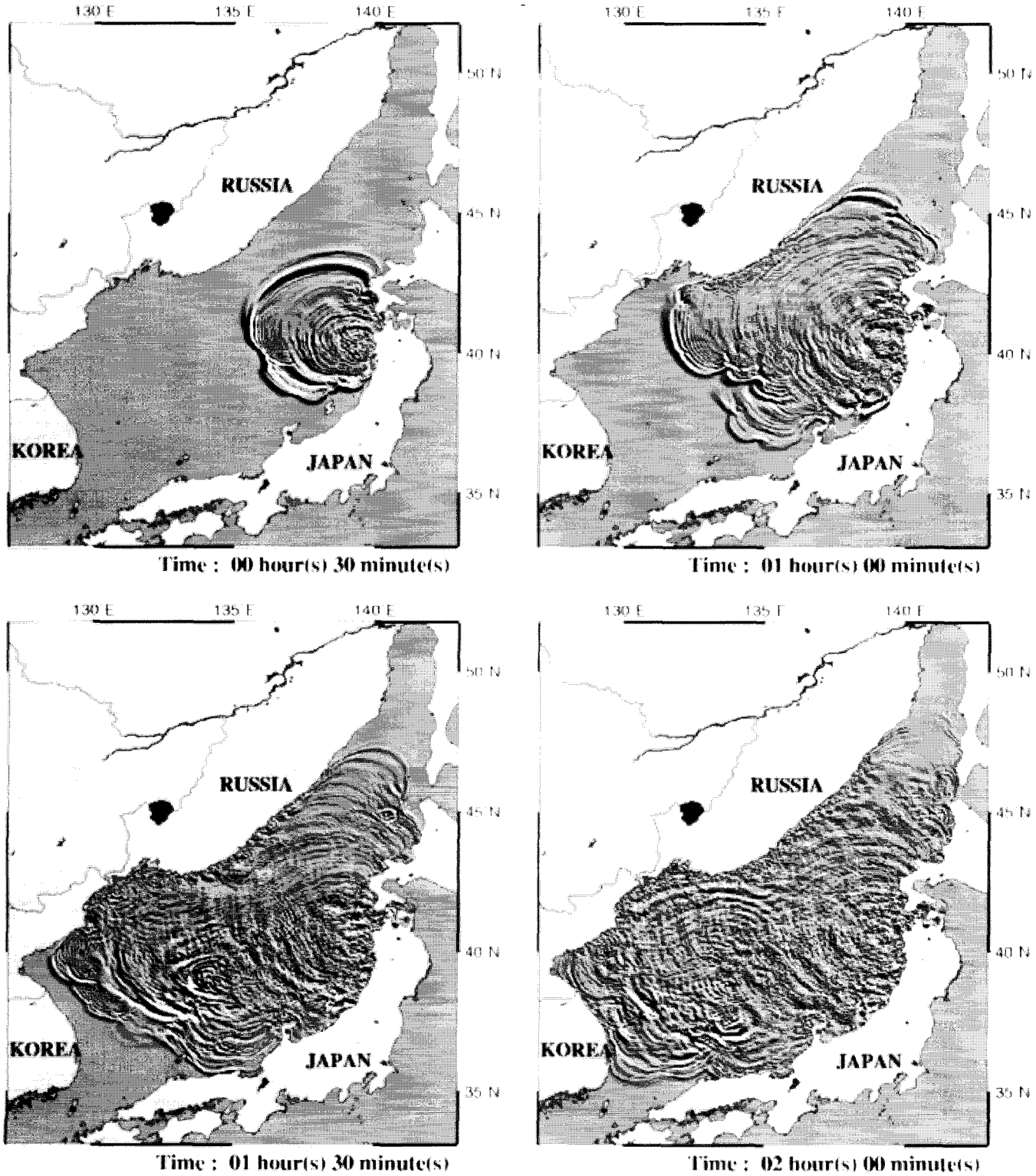

Fig. 13 Snapshots of images of computed sea elevation for tsunami on May 26, 1983 in the East(Japan) Sea

the observed data. As it can be seen, the agreement is well, and the log-normal curve is a good approximation of the real distribution function.

The snapshots of tsunami propagation from the source to the coast are shown in Fig. 13, which shows the general pattern of wave propagation in the East Sea. The characteristic tide-gauge records of tsunami at Mukho(37° 32'50"N, 129° 07'06"E) and Sokcho(38° 12'14"N, 128° 35'50"E) are presented in Fig. 14 and the calculated tide-gauge records of tsunami at the same points are shown in Fig. 15. As shown in Fig. 14, the first tsunami wave arrived in the mid-eastern coast of Korea(Mukho and Sokcho) at 13:40, May 26, 100minutes after the earthquake occurred in central East Sea at 11:59, May 26. The time series of simulation results(Fig. 15) also shows the arrival time of around 100~110 minutes, indicating that the accuracy of model performance is acceptable.

The numerical model is used to calculate tsunami run-up heights along the eastern coast of Korea, and computed data is presented in Fig. 16. Comparison of calculated and observed tsunami run-up height is given in Fig. 17. As it can be seen, the comparison is good for many coastal points and this shows good applicability for description of the real tsunami event.

Numerical results are also used to analyze the distribution function of tsunami run-up heights for different innermost subregions. The distribution function for each subregion and the comparison with the log-normal form is shown in Fig. 18. Distribution function in each sub-region(region 01 ~region 15) agrees very well with the log-normal form. However, subregion 11 shows slight discrepancy between distribution function and log-normal form. This deviation could be caused by the characteristic of local bathymetry in subregion 11. Further research would be needed to fully understand this feature.

The distribution function for the whole subregions is shown in Fig. 19. It is clearly seen that distribution functions tends to the log-normal form and represent a bythymetric features of the coastal zone. These numerical experiments confirm the theoretical hypothesis that real inhomogeneous bottom relief is a major factor determining the log-normal character of the distribution function.

4. Conclusion

In the present study, dynamic interfacing algorithms for parallel and inclined connecting boundaries are developed and applied to real tsunami situations. Numerical simulations of 1983 tsunami have shown a good agreement with the observed data in terms of the arrival time of the tsunami and maximum run-up heights along the eastern coast of Korea.

Calculations with different grid sizes demonstrate that the bottom irregularity in the coastal zone is a major factor influencing on the form of the distribution function and

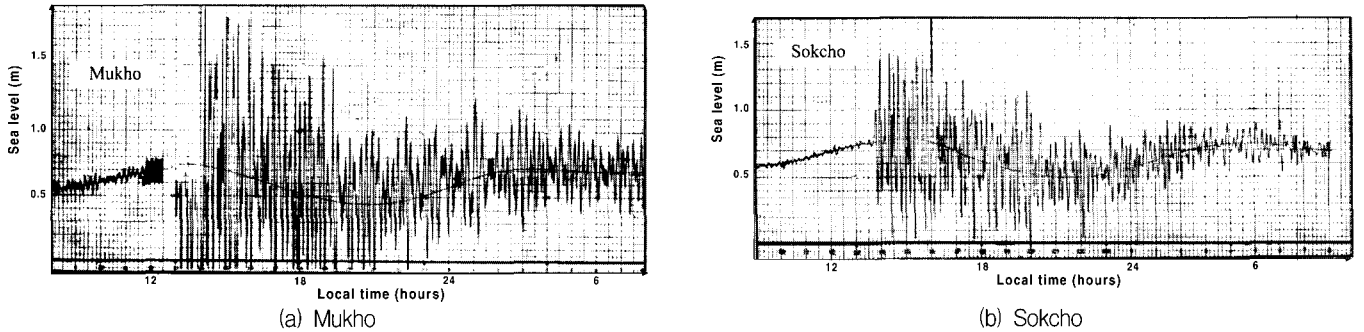

(a) Mukho (b) Sokcho

Fig. 14 Tide gauge records of the 1983 tsunami event at Mukho and Sokcho

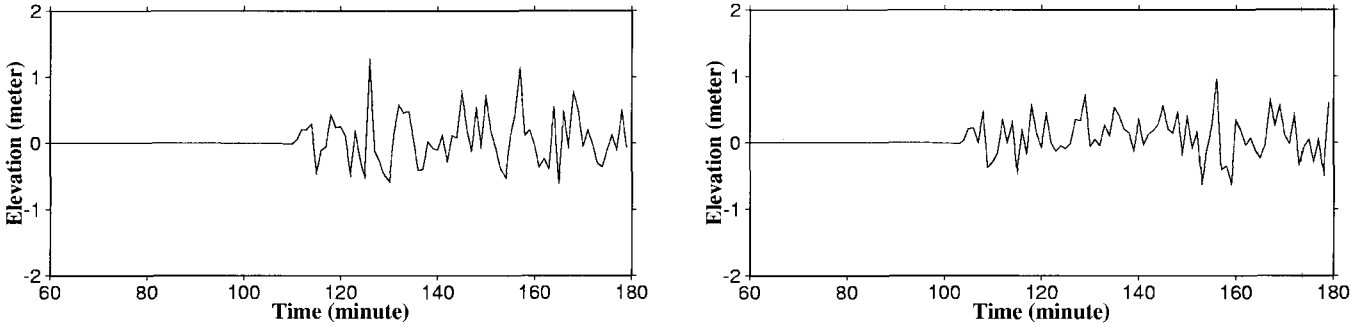

(a) Mukho (b) Sokcho

Fig. 15 Calculated tide gauge records of tsunami at the same points in Fig. 14

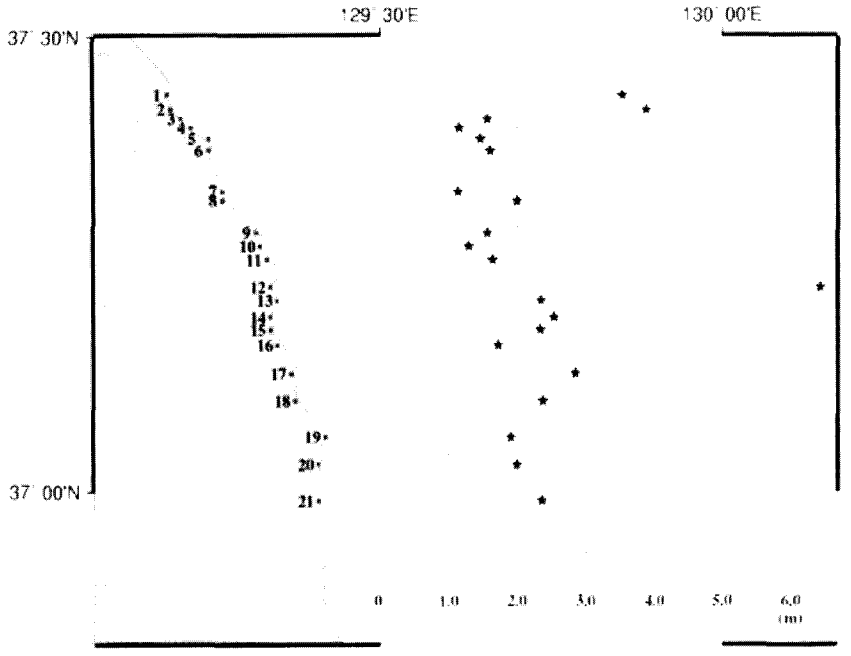

Tsunami Heights

Name of points	Height(meter)
1. Samchuk Port	3.54
2. Geunduk	3.89
3. Namapo	1.575
4. Gungchun Beach	1.16
5. Gungchun	1.47
6. Chogok	1.61
7. Yongwha Beach	1.14
8. Yongwha Port	2
9. Jangho Port	1.57
10. Galnam Port	1.3
11. Shinnam Port	1.65
12. Imwon Port	6.44
13. Biwha Port	2.35
14. NogokPort	2.54
15. Jakjin Port	2.34
16. Hosan Port	1.72
17. Nagok Port	2.85
18. Bugu Port	2.37
19. Chukbyun Port	1.91
20. Onyang Port	2.2
21. Eubnam Port	2.36

Fig. 16 Calculated tsunami run-up height along east Korean coast for the 1983 tsunami event

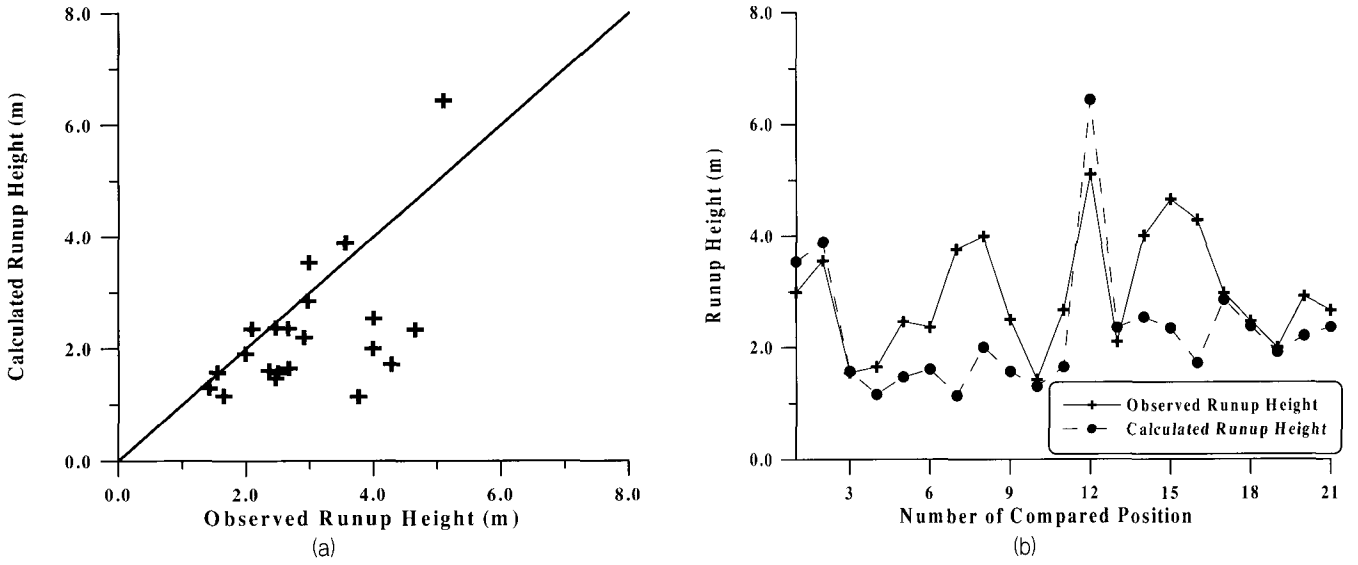

Fig. 17 Comparison of computed and observed runup heights on the 1983 tsunami

its closeness to the log-normal distribution. It is demonstrated that the distribution function for each subregion as well as for the whole summation of subregions is quite close to the log-normal form. These results confirm the theoretical idea of the form of the tsunami distribution function proposed by Van Dorn.[11]

In certain subregion the distribution function deviates from the log-normal form. Although the deviation is quite small, a further investigation would be needed to understand the cause of this difference.

Acknowledgements

This work was supported by the Korean Science and Engineering Foundation(KOSEF) through the Korea Earthquake Engineering Research Center(KEERC) at Seoul National University, and particularly(for EP) by Russian Fund for Basic Research.

References

1. Choi, B. H., Pelinovsky, E., Hong, S. J., and Woo, S. B., "Computation of tsunami in the East (Japan) Sea using dynamically interfaced nested model," *Pure and Applied Physics*, 2002, Accepted.
2. Murty, T., "Seismic sea waves-tsunamis," *Bull.*, No. 198, Dep. Fisheries, Canada, 1977, pp. 337.
3. Pelinovsky, E., "Nonlinear dynamics of tsunami," *Inst.*

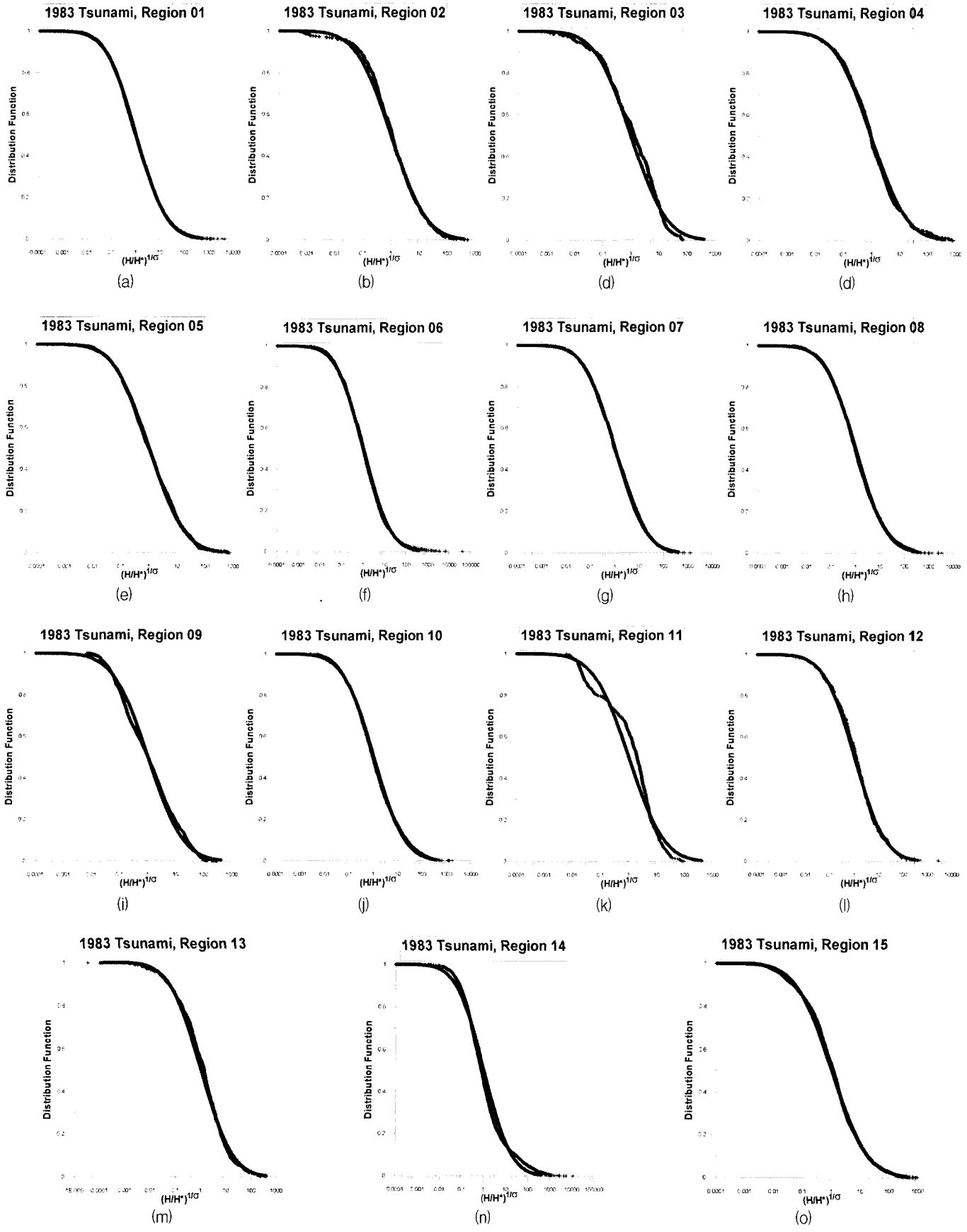

Fig. 18 The distribution function for each subregion and the comparison with the log-normal form

Appl. Phys., 1982, pp. 226.

4. Abbott, M. B., McCowan, A. D., and Warren, I. R., "Numerical modeling of free-surface flows that are two-dimensional in plan," In: Transport Models for Inland and Coastal Waters, Ed. H. B. Fisher, Academic Press, 1981, pp. 222-283.

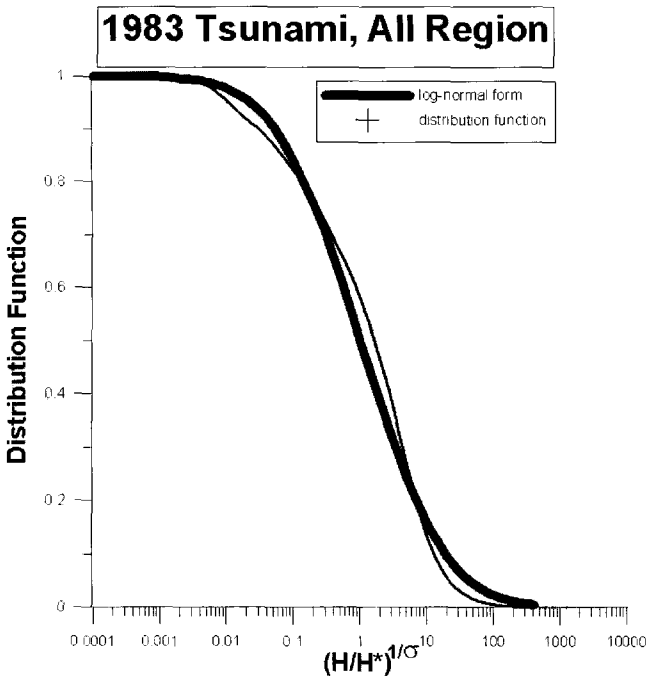

Fig. 19 The distribution function for the whole subregions and the comparison with the log-normal form

5. Liu, P. L. F., Cho, Y. S., Briggs, M. J., Kanoglu, U., and Synolakis, C. E., "Runup of solitary waves on a circular island," *J. Fluid Mech.*, Vol. 302, 1995, pp. 259-285.
6. Cho, Y. S. and Yoon, S. B., "A modified leap-frog scheme for linear shallow-water equations," *Coastal Engineering Journal*, Vol. 40, No. 2, pp. 191-205.
7. Aida, I., "A source models of the 1983 Nihonkai-earthquake tsunami," *Proceeding of 3rd United States-Japan Cooperative Program in Natural Resources Tsunami Workshop*, 1984, pp. 57-76.
8. Manshinha, L. and Smylie, D. E., "The displacement fields of inclined faults," *Bull. Amer. Seism. Soc.*, Vol. 61, No. 5, 1971, pp. 1433-1440.
9. Tsuji, Y. et al., "Report of the 1983 Nihonkai Chubu earthquake tsunami along the east coast of the Republic of Korea," *National Research Center for Disaster Prevention*, Japan, 1985, pp. 49-86.
10. NIDP, "Study on tsunami hazards mitigations along the Korean eastern coast(I)," *Report of NIDP(National Institute for Disaster Prevention)*, 1999, pp. 192.
11. Van Dorn, W. G., *Tsunamis*, In Advances in Hydroscience, Ed. V. T. Chow, Academic Press, London, Vol. 2, 1965, pp. 1-48.
12. Kajiura, K., "Some statistics related to observed tsunami heights along the coast of Japan," In: Tsunamis - Their Science and Engineering, Terra Pub., Tokyo, 1999, pp. 131-145.
13. Choi, B. H., Pelinovsky, E., Ryabov, I., and Hong, S. J., "Distribution function of tsunami wave heights," *Natural Hazards*, Vol. 25, No. 1, 2002, pp. 1-21.